Possible Flexural Wave Propagation Regimes in Periodic Beams

Nur Cristian Sangiorgio, **Joaquin Garcia-Suarez**,
Institute of Civil Engineering, École Polytechnique Fédérale de Lausanne (EPFL), CH 1015 Lausanne, Switzerland
Corresponding author: joaquin.garciasuarez@epfl.ch

Abstract

Flexural wave propagation in periodic beams has been the object of studies for decades and it remains an active field of research, particularly because of the possibility of generating bandgaps, i.e., frequency intervals at which wave propagation is not allowed. For three models of beams (Euler-Bernoulli, Rayleigh or Timoshenko), there exist two wave modes, and each one of them can be either propagating, evanescent (exponentially decaying) or decaying with oscillations. The present work establishes which combinations in mode character can emerge when the beam is assumed as infinitely periodic and the unit cell is piece-wise constant. Regardless of number of layers in the unit cell and material and cross-section properties, a priori guarantees on the wave propagation behavior are derived, showing that Euler–Bernoulli beams always feature an evanescent mode, while any combination of modes is possible for Rayleigh and Timoshenko, unless the design parameter space is constrained. Bloch's theorem for infinite media and spectral analysis of transfer matrices are the mathematical levers we use to derive the results, once the relation between eigenvalues of the transfer matrix and wave propagation is established. Our approach relies on leveraging the symplectic structure of the transfer matrices and the notion of "dominant eigenvalue". Practical consequences and the possible extension of the results towards continuous beam profiles are discussed. This work offers foundational results to guide bandgap optimization for flexural waves.

Keywords: Wave Propagation, Multi-Layered Media, Bandgap, Spectral Analysis, Waveguide

1 Introduction

Wave propagation in media composed of a periodically repeated structure, typically known as the *unit cell*, has been an active research area for decades (Bloch, 1929; Brillouin, 1953). When the number of repetitions of the unit cell is sufficiently high, boundary effects can be safely removed from the analysis, and the medium is modeled as infinitely periodic, as in Figure 1. One peculiarity of these systems is the possibility of generating frequency ranges where waves do not propagate, termed "bandgaps or "stop-bands" (as opposed to "passbands"), enabling the design of systems that act as filters for wave control purposes. Nowadays, given the interest around metamaterials and increased design opportunities offered by advanced manufacturing technologies, the topic has captured the attention of various scientific communities (Hussein et al., 2014; Price et al., 2022). Recent work on beam metamaterials for flexural-wave control (sometimes termed "waveguides") increasingly points toward multiphysics and programmability, with thermally reconfigurable metabeams (Zhang et al., 2024), actively tuned piezoelectric cells (Zhang et al., 2025), graded piezoelectric meta-beams for wave compression (Dai et al., 2024), and even time-varying elastic beams for temporal scattering and frequency conversion (Wang et al., 2025). At the same time, a complementary line of research shows that simpler piecewise-constant beam architectures remain highly relevant for applications (Liu and Hussein, 2011), e.g., alternating periodic waveguides can be optimized efficiently for targeted attenuation (Renno, 2025).

For a time-harmonic wave at frequency ω and a given set of defining parameters $\boldsymbol{\theta}$ (material properties, geometry, etc.) it is well known in the literature (Kittel, 2004) that flexural wave propagation depends on the four eigenvalues λ of an associated *transfer matrix* $\boldsymbol{T}(\omega;\boldsymbol{\theta})$. Consequently, the problem of bandgap

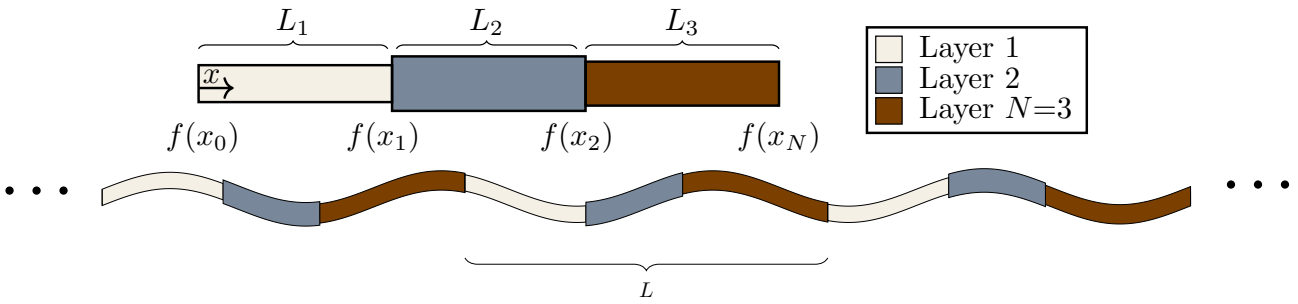

Figure 1: Reference model for flexural waves in infinite 1D multi-layered media. Unit cell with $N = 3$ layers, EI, ρA are constants within each layer.

design can be understood as choosing the proper $\boldsymbol{\theta}$ such that the associated transfer matrix has a spectrum that forbids wave propagation only at target frequencies.

In the context of periodic linear-elastic beams, it has firmly been established that to two pairs of flexural modes (each made up of a wave moving left and one moving right) can be present in the layered beam in steady state (Mead, 1975). A consequential contribution by Romeo and Luongo (2002) has analyzed the possible wave propagation regimes, i.e., the "types" of propagating waves and bandgaps that can coexist for the two modes, through the possible spectral configurations of the corresponding transfer matrices. There are four possibilities, arising from the eigenvalue structure: $\mathsf{Pass}-\mathsf{Pass}$ (two propagating waves for each mode; four complex unit-modulus eigenvalues), $\mathsf{Pass}-\mathsf{Stop}$ (one mode features propagating waves, the other one does not; two real eigenvalues plus two unitary eigenvalues), $\mathsf{Stop}-\mathsf{Stop}$ (four exponentially-decaying waves; two real eigenvalues plus two unitary complex eigenvalues), and so-called $\mathsf{Complex}$ (four waves that decay exponentially as they propagate; four complex eigenvalues).

For different beam models and under the assumptions previously mentioned, there are two convenient *matrix invariants* $I_{1,2}$ (Carta and Brun, 2015) whose relative value define the different wave propagating regimes for the two modes, as in Figure 2. $I_1(\omega;\boldsymbol{\theta}) = \text{trace}(\boldsymbol{T}(\omega;\boldsymbol{\theta}))$ is but the trace of the transfer matrix (the sum of all eigenvalues), while the second invariant $I_2(\omega;\boldsymbol{\theta}) = 1/2(\text{trace}(\boldsymbol{T}(\omega;\boldsymbol{\theta}))^2 - \text{trace}(\boldsymbol{T}^2(\omega;\boldsymbol{\theta}))$ is a more complicated function of the eigenvalues. To lighten the notation, from now on we will remove the explicit dependence on $\boldsymbol{\theta}$.

Once a beam model is chosen and the corresponding physical parameters $\boldsymbol{\theta}$ in the *unit cell*, the generation of bandgaps/stopbands can be studied by means of trajectories, parametrized by ω, in the $I_1 - I_2$ space (Romeo and Luongo, 2002; Carta and Brun, 2015); at different frequencies a trajectory can move between different regions, indicating that the nature of at least one mode has changed (i.e., it has entered a frequency range corresponding to a stopband). Assuming a priori that any combination of material and geometrical properties was possible (i.e., total freedom in choosing $\boldsymbol{\theta}$), some relevant questions on bandgaps for flexural waves in beams include:

1. Is there a combination of parameters that ensures reaching a given combination in mode natures? This is equivalent to asking: which regions of the $I_1 - I_2$ can a trajectory access?

2. How do the results change based on the beam modeling assumptions? I.e., can we extrapolate bandgap engineering insights from Euler-Bernoulli beams to Rayleigh or Timoshenko beams?

3. Out of the four eigenvalues that define the spectrum of the beam transfer matrices, which eigenvalues control the transition between different regions and thus the generation of bandgaps?

These questions, to the best of our knowledge, still lack a definitive answer. In this manuscript, three reference beam models will be addressed, respectively the Timoshenko model, the Rayleigh model, derived from the previous one by neglecting shear deformation, and the Euler–Bernoulli beam, as a limit case of Rayleigh for negligible rotary inertia. The three are considered under free vibrations, namely without

external loads, moments and in absence of foundations. Also, only multi-layered media are taken into account, that is the case of piecewise constant physical properties of the beam inside each repeated unit cell, defining adjacent homogeneous layers, as in Figure 1.

Several results (Lim and Xu, 2010; Doyle, 2020) are available in the literature concerning the spectral analysis of constant cross-section beams and bi-layered structures ($N = 2$ homogeneous layers per unit cell). Indeed, for bi-layered Euler–Bernoulli beams, some examples for which bandgaps can be determined only by one specific pair of reciprocal eigenvalues of the transfer matrix, or where only the $\mathsf{Pass}-\mathsf{Pass}$ and $\mathsf{Pass}-\mathsf{Stop}$ regimes can occur, can be found in Lee et al. (1990) and Carta and Brun (2015). However, for multi-layered media with $N > 2$ layers, we have not found explicit investigation of spectral properties of transfer matrices. The objective of this work is thus to deliver a number of general results for any arbitrary number of layers, $N \geq 2$, regardless of the choice of the beam physical parameters, for the three most common beam models (Euler-Bernoulli, Rayleigh and Timoshenko).

The structure of the paper is as follows: Section 2 illustrates the derivation of a transfer matrix using Euler–Bernoulli beams (the other two types are addressed by adding to this baseline case). Also, the relevant theoretical background for the understanding of bandgaps for flexural waves in beams is provided. In Section 3 the research methodology adopted is presented, explaining how the notion of invariance of the spectrum up to similarity transformations has been used to derive spectral insights for Euler–Bernoulli beams. Section 4 showcases the outcome results for the three beam models considered, highlighting how each variation in the model assumptions affects the trajectories in the $I_1 - I_2$ space and the possibility of attaining certain bandgaps. Section 5 discusses previous work in light of the new results, as well as the possibility of extending those beyond the multi-layered assumption. We close with final remarks and perspectives for future work in Section 6. We have striven to make the paper self-contained, thus we have decided to provide extra mathematical background (definitions, statement of theorems extracted from the literature, formal proofs) in a Supplementary Material file.

2 Background: Governing Equations

2.1 The keystone case: transfer matrices for Euler–Bernoulli beams

Consider an Euler–Bernoulli beam undergoing free vibration. The longitudinal coordinate along the axis of the beam is x, the transverse displacement $w(x,t)$, the rotation of the cross-section $\phi(x,t)$, the shear force at each cross-section $V(x,t)$, and the bending moment $M(x,t)$. They are related through:

$$V(x,t) = -\frac{\partial M(x,t)}{\partial x}\,, \quad M(x,t) = EI(x)\frac{\partial \phi(x,t)}{\partial x}\,, \quad \frac{\partial w(x,t)}{\partial x} - \phi(x,t) = 0\,, \tag{1}$$

where EI denote Young's modulus times the moment of inertia of the cross-section. In addition, balance of linear momentum projected onto the transverse direction (in absence of distributed loads):

$$\frac{\partial^2}{\partial x^2}\left(EI(x)\,\frac{\partial^2 w(x,t)}{\partial x^2}\right) + \rho A(x)\,\frac{\partial^2 w(x,t)}{\partial t^2} = 0, \tag{2}$$

with ρA representing the linear density (volumetric density ρ times the cross-section area A). Assuming harmonic time evolution, we can write $w(x,t) = \hat{w}(x)e^{i\omega t}$, $V(x,t) = \hat{V}(x)e^{i\omega t}$ and $M(x,t) = \hat{M}(x)e^{i\omega t}$, with angular frequency ω, the prior equations become

$$\hat{V}(x) = -\frac{d\hat{M}(x)}{dx}\,, \quad \hat{M}(x) = EI(x)\frac{d\hat{\phi}(x)}{dx}\,, \quad \hat{\phi}(x) = \frac{d\hat{w}(x)}{dx}\,, \quad \frac{d^2}{dx^2}(EI(x)\,\frac{d^2\hat{w}}{dx^2}) = \rho A(x)\,\omega^2\,\hat{w}\,. \tag{3}$$

These equations can be recast as a first-order ODE system:

$$\frac{d}{dx}\boldsymbol{f}(x) = \boldsymbol{H}(x)\boldsymbol{f}(x)\,, \tag{4}$$

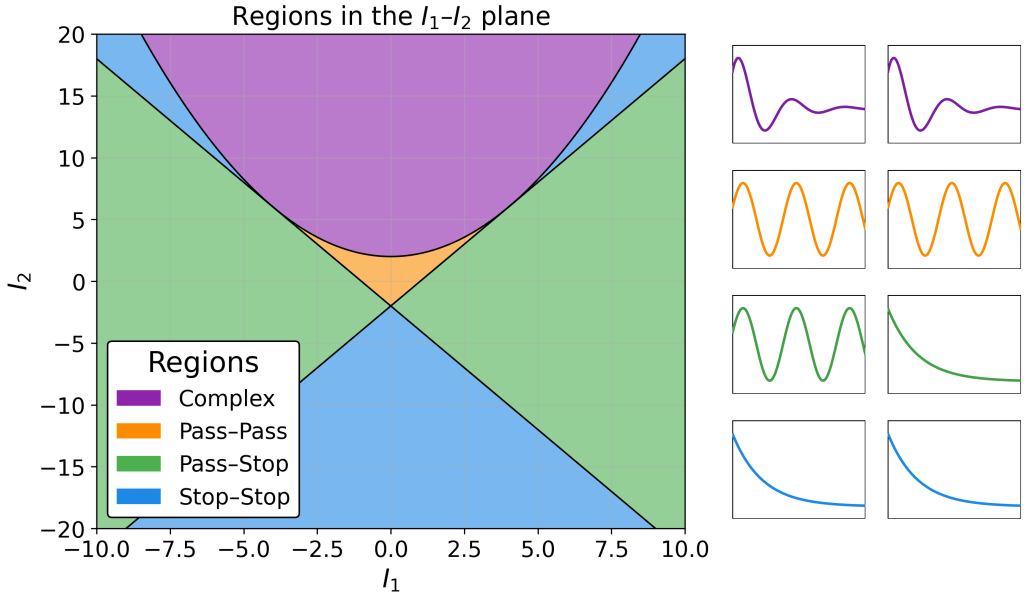

Figure 2: Regions on the $I_1 - I_2$ plane to classify all possible propagation mode configurations (left) and the two mode configurations for each region (right) (Romeo and Luongo, 2002), using the same colors. The "Stop-Stop" region (blue) corresponds to stopbands for both modes (both display imaginary wavenumbers) and is associated with two real reciprocal pairs of eigenvalues. The "Pass − Stop" region (green) corresponds to one passband and one stopband (one real and one imaginary wavenumber) and is associated with one reciprocal pair of eigenvalues (stopband) and one complex-conjugate unitary pair (passband). The "Pass − Pass" region (orange) corresponds to two passbands (two real wavenumbers) and is associated with two complex-conjugate unitary pairs of eigenvalues. The "Complex" region (purple) corresponds to the two modes propagating and being damped simultaneously (two complex wavenumbers, not necessarily unitary) and is associated with four complex eigenvalues.

by introducing the *state vector* $\boldsymbol{f}(x)$(Leckie and Pestel, 1960) and the *Hamiltonian* matrix $\boldsymbol{H}(x)$ (Stephen, 2006), which are

$$\boldsymbol{f}(x) := \begin{bmatrix} \hat{w} \\ \hat{\phi} \\ -\hat{V} \\ \hat{M} \end{bmatrix}, \qquad \boldsymbol{H}(x) := \begin{bmatrix} 0 & 1 & 0 & 0 \\ 0 & 0 & 0 & (EI(x))^{-1} \\ \rho A(x)\omega^2 & 0 & 0 & 0 \\ 0 & 0 & 1 & 0 \end{bmatrix}. \tag{5}$$

Table 1 presents $\boldsymbol{H}(x)$ for the Rayleigh beam model (which accounts for rotary inertia) and Timoshenko's (also accounts in addition for the coupling between shear and bending deformation).

Rayleigh	**Timoshenko**
$\begin{bmatrix} 0 & 1 & 0 & 0 \\ 0 & 0 & 0 & (EI)^{-1} \\ \rho A\omega^2 & 0 & 0 & 0 \\ 0 & \boxed{-\omega^2\rho I} & 1 & 0 \end{bmatrix}$	$\begin{bmatrix} 0 & 1 & \boxed{(-\kappa GA)^{-1}} & 0 \\ 0 & 0 & 0 & (EI)^{-1} \\ \rho A\omega^2 & 0 & 0 & 0 \\ 0 & \boxed{-\omega^2\rho I} & 1 & 0 \end{bmatrix}$

Table 1: The Hamiltonian matrices for Rayleigh and Timoshenko beam models. The terms added to the Euler-Bernouilli matrix are boxed for clarity. κ is the shear factor (Timoshenko, 1930).

We have made some deliberate choices as to signs to ensure that all the entries of $\boldsymbol{H}(x)$ for Euler-Bernoulli beams are strictly positive, eq. (5).

By assuming an N-layered piecewise-constant profile of the physical properties with $\rho = \rho_n$ and $EI = E_n I_n$ constants over lengths $L_n := x_n - x_{n-1}$ and $L = \sum_{n=1}^{N} L_n$ (total length of the unit cell) as in Figure 1, it holds true that

$$\boldsymbol{f}(x_n) = \boldsymbol{T}_n \boldsymbol{f}(x_{n-1}),$$

$$\boldsymbol{T}_n := e^{L_n \boldsymbol{H}_n} = \frac{1}{2} \begin{bmatrix} \cosh\zeta + \cos\zeta & \frac{1}{k_n}(\sinh\zeta + \sin\zeta) & \frac{\alpha_n}{k_n}(\sinh\zeta - \sin\zeta) & \alpha_n(\cosh\zeta - \cos\zeta) \\ k_n(\sinh\zeta - \sin\zeta) & \cosh\zeta + \cos\zeta & \alpha_n(\cosh\zeta - \cos\zeta) & \alpha_n k_n(\sinh\zeta + \sin\zeta) \\ \frac{k_n}{\alpha_n}(\sinh\zeta + \sin\zeta) & \frac{1}{\alpha_n}(\cosh\zeta - \cos\zeta) & \cosh\zeta + \cos\zeta & k_n(\sinh\zeta - \sin\zeta) \\ \frac{1}{\alpha_n}(\cosh\zeta - \cos\zeta) & \frac{1}{k_n\alpha_n}(\sinh\zeta - \sin\zeta) & \frac{1}{k_n}(\sinh\zeta + \sin\zeta) & \cosh\zeta + \cos\zeta \end{bmatrix}, \tag{6}$$

where the wavenumber in each homogeneous layer, k_n, appears along with other factors:

$$k_n = \left(\frac{\rho_n A_n(x)\,\omega^2}{E_n I_n(x)}\right)^{1/4}, \qquad \zeta = k_n L_n, \qquad \alpha_n = \frac{1}{\sqrt{E_n I_n(x)\,\rho_n A_n(x)\,\omega^2}}. \tag{7}$$

$\boldsymbol{T}_n$ itself is known as *transfer matrices* (it transfers the fields in the state vector $\boldsymbol{f}$ from x_n to $x_{n+1} = x_n + L_n$). They are defined through the matrix exponential operator applied to the Hamiltonian matrix, and happen to be elements of the real symplectic group (Stephen, 2006; Hall, 2015). For our purposes, symplecticity means that these matrices always have determinant one and that its eigenvalues necessarily come in reciprocal pairs (i.e., as a consequence of the form of their characteristic polynomial, if λ_1 and λ_2 are eigenvalues, so are $1/\lambda_1$ and $1/\lambda_2$). Even if the physical properties $\rho A(x)$ and $EI(x)$ jump at the interfaces of adjacent layers due to the piecewise continuous profile, a physical solution is guaranteed by enforcing the continuity of the variables in the state vector at interfaces, which means $\boldsymbol{f}(x_n^-) = \boldsymbol{f}(x_n^+)$ at positions x_n. It follows that

$$\boldsymbol{f}(x_N) = \boldsymbol{T}\,\boldsymbol{f}(x_0), \qquad \boldsymbol{T} := \boldsymbol{T}_N \boldsymbol{T}_{N-1} \cdots \boldsymbol{T}_2 \boldsymbol{T}_1. \tag{8}$$

Since the product of symplectic matrices remains symplectic (Hall, 2015), the global matrix $\boldsymbol{T}$ is guaranteed to keep the aforementioned properties (Carta and Brun, 2015).

Finally, note that the parameter vector $\boldsymbol{\theta}$ mentioned in the introduction can be expressed, for the Euler-Bernoulli case, as $\boldsymbol{\theta} = \{L_n, A_n, I_n, E_n, \rho_n\}_{i=1}^{N}$, i.e., it contains the length of each layer, its cross-section area and inertia, as well as its material stiffness and density. Should we want to design a unit cell featuring a bandgap over a certain frequency range, these are all the knobs to turn.

2.2 Bandgaps for flexural waves

We begin by recapitulating how flexural wave propagation problems can be studied through transfer matrices. In particular, Euler–Bernoulli, Rayleigh and Timoshenko beams are such that the associated transfer matrices belong to the symplectic group (i.e., all of them have unitary determinant and eigenvalues come in complex-reciprocal pairs). Given an infinite beam with periodic unit cell of length L, it follows from Bloch's theorem that the propagation along x of flexural waves depends on the eigenvalues $\lambda(\omega)$ of the corresponding transfer matrix $\boldsymbol{T}(\omega)$ (introducing the phase accumulated over the whole unit cell, kL):

$$\boldsymbol{f}(x_N) = \boldsymbol{T}(\omega)\boldsymbol{f}(x_N) = e^{\mathrm{i}kL}\boldsymbol{f}(x_N) \Rightarrow \lambda(\omega) := e^{ikL}\,, \tag{9}$$

so a wave at frequency ω can propagate only when the wavenumber k is real, or equivalently $\boldsymbol{T}$ admits an eigenvalue with $|\lambda| = 1$, i.e., on the unit circle (Romeo and Luongo, 2002; Carta and Brun, 2015). The function $k = k(\omega)$ is termed *dispersion relation* in the literature (Kittel, 2004). The symplectic structure of $\boldsymbol{T}$ implies that its characteristic polynomial depends only on the two *invariants* I_1 and I_2 as

$$p_T(\lambda) := \det(\lambda\boldsymbol{I} - \boldsymbol{T}) = \lambda^4 - I_1\lambda^3 + I_2\lambda^2 - I_1\lambda + 1, \tag{10}$$

where (Horn and Johnson, 2012; Carta and Brun, 2015)

$$I_1(\boldsymbol{T}) = \mathrm{trace}(\boldsymbol{T}) = \lambda_1 + \frac{1}{\lambda_1} + \lambda_2 + \frac{1}{\lambda_2}\,, \tag{11a}$$

$$I_2(\boldsymbol{T}) = \frac{1}{2}(\mathrm{trace}(\boldsymbol{T})^2 - \mathrm{trace}(\boldsymbol{T}^2)) = 2 + \left(\lambda_1 + \frac{1}{\lambda_1}\right)\left(\lambda_2 + \frac{1}{\lambda_2}\right)\,, \tag{11b}$$

where it has been used that the equation $p_T(\lambda) = 0$ admits always two pairs of solutions (the spectrum of $\boldsymbol{T}$) of the form $\lambda_1, \lambda_1^{-1}, \lambda_2, \lambda_2^{-1}$ (the subscripts here should not to be confused with the two invariants). It is convenient to introduce $y_{1,2} := \lambda_{1,2} + \lambda_{1,2}^{-1} = 2\cos(k_{1,2}L)$ (the cosine has to be understood as taking any generic complex argument) which consolidates the right-going and left-going waves belonging to one of the modes in a single variable. Thus, understanding each y means understanding each mode.

Instead of analyzing the four solutions of the biquadratic equation $p_T(\lambda) = 0$, the spectrum can be determined (Romeo, 2012) from the two the solutions of a quadratic equation by substituting y into eq. (10),

$$y^2 - I_1 y + (I_2 - 2) = 0, \tag{12}$$

which leads to two pairs of eigenvalues of the problem $y_{1,2}$ as

$$y_{1,2} = \frac{1}{2}\left(I_1 \pm \sqrt{I_1^2 - 4I_2 + 8}\right), \tag{13}$$

and consequently – recall that $y = 2\cos(kL)$ – the two "branches" of dispersion relations are

$$k_{1,2}L = \arccos\left(\frac{y_{1,2}}{2}\right)\,. \tag{14}$$

It follows that the wavenumber k is real and the corresponding eigenvalues are complex on the unit circle whenever

$$y \in \mathbb{R}, \quad |y| \leq 2 \tag{15}$$

while real distinct reciprocal eigenvalues occur when

$$y \in \mathbb{R}, \quad |y| > 2\,. \tag{16}$$

See that, having y, one recovers the eigenvalues from

$$\lambda^2 - y\lambda + 1 = 0 \Rightarrow \lambda = \frac{y}{2} \pm \sqrt{\left(\frac{y}{2}\right)^2 - 1}\,. \tag{17}$$

Let us recall Figure 2 at this point. See how the different combinations of $y_{1,2}$ in terms of eqs. (15) and (16) define the possible combinations of stop or pass bands (each colored region) for the modes in terms of I_1 and I_2, according to eq. (13). Moreover, once we fix the design parameters $\boldsymbol{\theta}$, I_1 and I_2 still depend on frequency, so as we sweep over ω we draw a trajectory in the $I_1 - I_2$ plane; a small variation in ω can change the nature of a solution of eq. (13) and the magnitudes of y, recall eqs. (15) and (16), meaning that we cross from region in the plot to an adjacent one. Among other things, this is a way to understand how bandgaps open and close for different modes.

In Romeo and Luongo (2002), a thorough analysis of the specific spectral configurations of the transfer matrices as a function of the invariants is performed, determining different wave propagation regimes. Correspondingly, for each value of frequency ω, one among the following four main cases can be identified once determined the invariants $I_{1,2}$, as shown in Figure 2:

1. The $\mathsf{Stop} - \mathsf{Stop}$ region, where no wave propagation can occur, associated with two real reciprocal pairs of eigenvalues. For some real values α, the two wavenumbers $k_{1,2}$ admit the form $k = \pm i\alpha$ (positive eigenvalues) or $k = \pi \pm i\alpha$ (negative eigenvalues).

2. The $\mathsf{Pass} - \mathsf{Stop}$ region, where only one propagating wave mode occurs. It admits one real reciprocal pair of eigenvalues and one complex conjugate pair on the unit circle. The wavenumbers $k_{1,2}$ are such that one is real and the other still admits the form $\pm i\alpha$ or $\pi \pm i\alpha$ for some real α.

3. The $\mathsf{Pass} - \mathsf{Pass}$ region, where two propagation modes occur at the same time, and two pairs of complex conjugate eigenvalues are on the unit circle with $k_{1,2}$ real

4. The $\mathsf{Complex}$ region, where damped waves occur, and there are four complex eigenvalues not on the unit circle, given by $k_{1,2}$ complex conjugate with nonzero real part.

If the $\mathsf{Complex}$ case is excluded, for both λ on the unit circle and real by definition $y \in \mathbb{R}$, and from the equation of the parabolic boundary of the Complex region (Romeo and Luongo, 2002) it follows that the quantity under square root in eq. (13) is nonnegative, which implies $y_1 \leq y_2$.

3 Methodology: Spectral Invariance and Dominant Eigenvalue

Our methodology relies on a cascade of five key observations (Berman and Plemmons, 1994):

1. For the beam models considered, the continuity condition at interfaces of adjacent layers (of displacement, slope, bending moment, and shear force) is not affected by a sign variation in the entries of the state vector $\boldsymbol{f}(x)$; it just means we are multiplying the corresponding equation by -1 and/or absorbing signs in the definitions of variables. Importantly, this arbitrariness does not affect the eigenvalues of $\boldsymbol{H}_n$, i.e., moving signs in the definition of variables or in members of the equations does not affect the invariants $I_{1,2}$ (this, in mathematical terms, would be stated as "similarity transformations do not change matrix spectra"). Hence, whatever we say about the spectrum of $\boldsymbol{H}_n$ as presented in eq. (3) (all entries greater or equal to zero) is independent of those sign permutations.

2. For Euler-Bernouilli beams, $\boldsymbol{H}_n$ as presented in eq. (3) is – in the strict mathematical sense – both *nonnegative* (all entries greater or equal to zero) and *irreducible* (there are no permutations that render the matrix upper-triangular , see Berman and Plemmons (1994)).

3. From the latter, given that $L_n > 0$, it follows that the exponential matrix $\boldsymbol{T}_n = \exp(\boldsymbol{H}_n L_n)$ is *positive*, all entries of $\boldsymbol{T}_n$ are strictly greater than zero.

4. It follows, invoking Perron-Frobenius theorem (Berman and Plemmons, 1994), that $\boldsymbol{T}_n$ has a *simple, real, positive, strictly dominant* eigenvalue. "Strictly dominant" means that its absolute value is strictly greater than all other three eigenvalues. The wave propagation implication of this will be pondered in next section.

5. The product $\boldsymbol{T} = \boldsymbol{T}_N \dots \boldsymbol{T}_n \dots \boldsymbol{T}_1$ inherits the property from individual matrices, i.e., it also has a simple, real, positive, strictly dominant eigenvalue, which we will call $\lambda^\star$, eq. (16).

This last result can be proved, primarily, from the expansion of the matrix exponential, using the fact that all possible addends in the expansion have to remain positive due to the matrix exponentiated being positive and irreducible. Even though this proof can be found in the literature, we reproduce it in the Supplementary Material, using the same notation as in this text. These results and definitions have been consulted in Berman and Plemmons (1994).

4 Results: Bandgap Possibilities

4.1 Euler-Bernoulli: either no mode propagates or just one does

The matrices $\boldsymbol{H}$ and $\boldsymbol{T}$ for Euler-Bernoulli beams, eqs. (5) and (6), meet all the requirements in the prior section; thus $\boldsymbol{T}$ has a simple, positive, real, dominant eigenvalue, $\lambda^\star$. Moreover, the fact that $\boldsymbol{T}$ is symplectic means that $1/\lambda^\star$ is also an eigenvalue. This is enough to state that

- One "dominant" propagation mode, the one associate to the pair $\{\lambda^\star, 1/\lambda^\star\}$, is always evanescent. This follows directly from $\lambda^\star$ being real and positive, thus $y_2 = y^\star = \lambda^\star + 1/\lambda^\star > 2$.

- The other propagation mode (the other pair of eigenvalues, let us call them, $\{\lambda^\dagger, 1/\lambda^\dagger\}$) can be real or complex. In the real case, one eigenvalue must be the inverse of the other; in the Complex case, they must be Complex conjugates.

- Since the dominant mode contains always two real eigenvalues, it follows from eq. (13) that the other $y_1 = y^\dagger = \lambda^\dagger + 1/\lambda^\dagger$ (where the dagger notation is used for convenience and has nothing to do with complex conjugation) has to be real as well, so,

  (a) either these $\lambda^\dagger$ and $1/\lambda^\dagger$ are real and reciprocal,

  (b) or they are Complex conjugates in the unit circle to ensure that their sum $y^\dagger = \lambda^\dagger + 1/\lambda^\dagger = e^{\mathrm{i}kL} + e^{-\mathrm{i}kL} = 2\cos(kL)$ is real as well despite the addends being complex.

- In wave propagation terms, this means that the other non-dominant mode can only be either also evanescent (real eigenvalues), or propagating (unitary Complex eigenvalues).

- In conclusion: in Euler-Bernoulli beams, regardless of frequency range ω or material and geometrical parameters $\boldsymbol{\theta}$, the two modes cannot propagate simultaneously – only the non-dominant can or not, but it cannot decay as it oscillates because, if complex, both eigenvalues necessarily have unit modulus. Equivalently, the regions Pass − Pass and Complex in the $I_1 - I_2$ diagram are closed to modes in Euler-Bernoulli beams, always.

To gain further insight, regard the four eigenvalue diagrams in Figure 3. It can be noted how the dominant eigenvalue $\lambda^\star$, largest in modulus and represented in red together with its reciprocal, defines a region delimited through a yellow circle in which the other eigenvalues associated with the non-dominant pair of eigenvalues, respectively green or blue, are constrained. The restriction imposed by the yellow

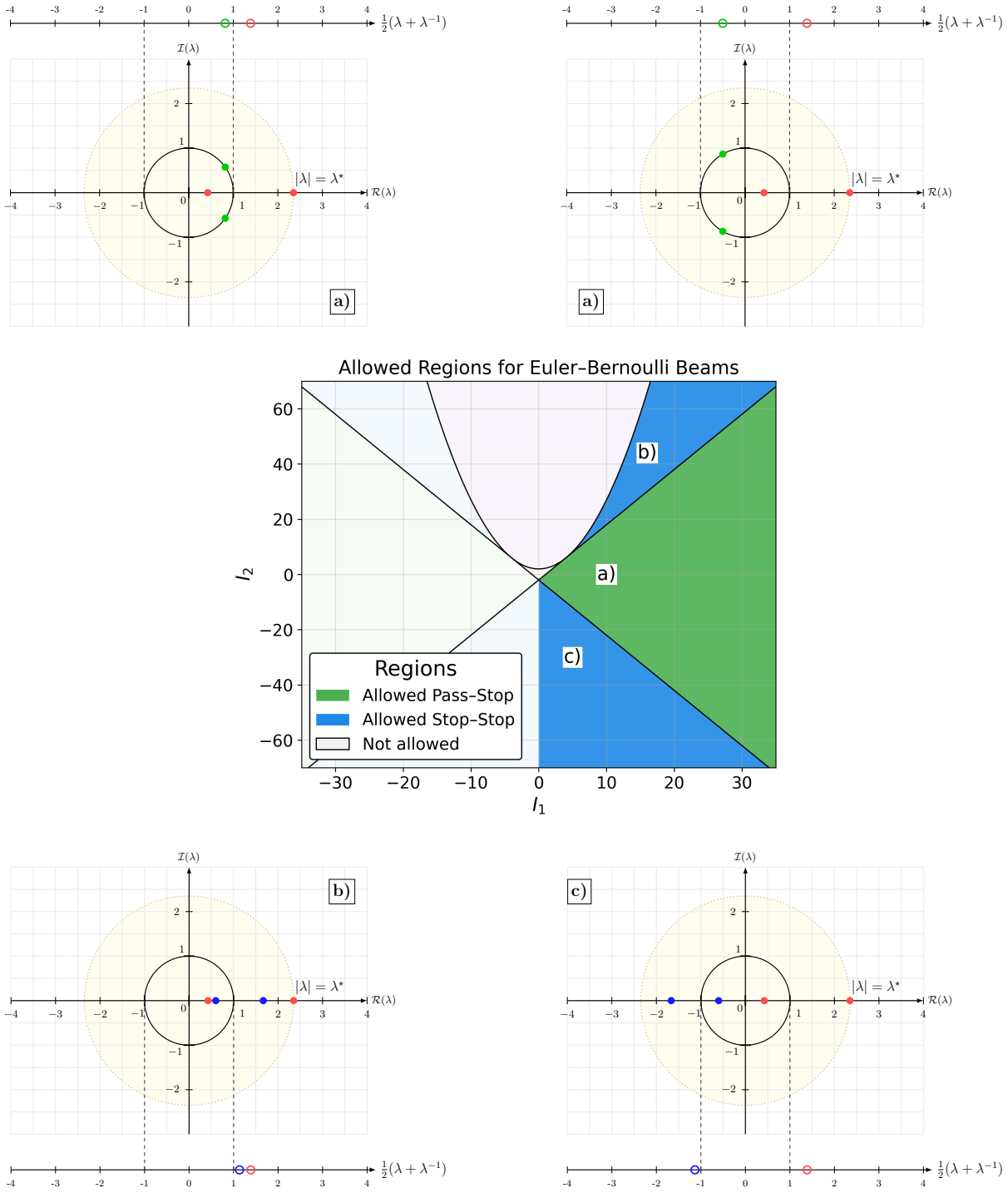

Figure 3: Representative spectral plots for multi-layered Euler-Bernoulli beams. Top: two representative spectral configurations of transfer matrices in multi-layered beams corresponding to one stopband and one passband. The associated region in the $I_1 - I_2$ space is a). Middle: the corresponding regions on the I_1-I_2 plane (regions not accessible to Euler-Bernoulli beams are transparent), highlighting where configurations a), b) and c) belong to. Bottom: two representative spectral configurations of transfer matrices in multi-layered beams corresponding to two stopbands. The associated regions in the $I_1 - I_2$ space are b) and c).

circle implies that y_1 can never be "negative enough" to exit that region, implying that the strongest condition holds true

$$y^\star > 2\,, \qquad |y^\dagger| < y^\star \qquad \Rightarrow \qquad I_1 = \mathrm{trace}(\boldsymbol{T}) = y^\star + y^\dagger > 0\,, \tag{18}$$

by definition of trace as sum of the eigenvalues.

In terms of wavenumbers and referencing everything to the $I_1 - I_2$ plane and trajectories therein, using $k^\star$ and $k^\dagger$ to denote the wavenumber of the dominant and non-dominant mode, respectively. we can equivalently state:

- The branch of dispersion relation $k^\dagger(\omega)$ can be either real or imaginary, controlling the generation of bandgaps, while $k^\star(\omega)$ is always imaginary, determining a non-propagating dominant wave mode.
- No trajectory can enter the Complex or Pass − Pass regimes; only the Stop-Stop and Pass-Stop regimes can occur under the condition $I_1 > 0$.
- There exists a scalar function

$$\eta(\omega) := \frac{|y^\dagger|}{2} = \frac{1}{4}|I_1(\omega) - \sqrt{I_1^2(\omega) - 4I_2(\omega) + 8}| \tag{19}$$

  such that if and only if $\eta > 1$ then the pair $\{I_1(\omega), I_2(\omega)\}$ belongs to the Stop-Stop region, i.e., k_1 is imaginary and a bandgap occurs. Thus, this function is the analogue of the half-trace function used to analyze bandgaps in 1D wave systems (García-Suárez, 2022; González-Carbajal et al., 2025), but for the non-dominant mode of flexural waves in Euler-Bernoulli beams.

Conversely, we will next show that in Rayleigh and Timoshenko beams the trajectories can reach any region in the $I_1 - I_2$ space, and an analogous function $\eta(\omega)$ cannot exist.

4.2 Timoshenko and Rayleigh: all mode combinations are possible

How do the results derived for Euler–Bernoulli change for different modeling assumptions? The Hamiltonian matrix for Euler-Bernouilli, see eq. (5), can be made to have only positive entries by signs permutations (similarity transformations). This is equivalent to $\boldsymbol{H}$ being both *irreducible* and *nonnegative*, the two necessary conditions to conclude the existence of a dominant eigenvalue which is real and positive. The second condition does not hold for the Rayleigh and Timoshenko beams, as the extra terms (highlighted in Table 1) introduce negative entries whose sign cannot be "removed" by similarity transformations. So:

- Which regions in the $I_1 - I_2$ space can be accessed by these beams? Since no eigenvalue has to be necessarily real, the Complex region (four Complex eigenvalues) is a priori open to some combination of frequency and design parameters. Moreover, the bounding condition eq. (18) does not have to hold, so we can enter regions in which either $|y|$ is greater, so the Pass − Pass is also open a priori. In Figures 4 to 7 we verified that those regions are indeed reachable, plotting some trajectories in the $I_1 - I_2$ (for fixed $\boldsymbol{\theta}$). Already by adding rotary inertia, the multi-layered Rayleigh model reaches the four propagation regimes. The same holds true for the Timoshenko model, see Figure 7, as it adds bending-shear coupling on top of rotary inertia.
- Is there still a single pair of eigenvalues controlling bandgaps? Since the classification of modes as $y^\dagger$ and $y^\star$ is not possible, the function η, eq. (19), cannot even be defined. It follows that, while considering shear deformation effects and rotary inertia in Rayleigh and Timoshenko beams, the existence of a single scalar function $\eta(\omega)$ determining the presence of bandgaps is not possible, as both pairs of reciprocal eigenvalues need to be evaluated.

Furthermore, a randomized sampling of combinations of frequencies and medium parameters over a large number of configurations for all the three models introduced in this work, both under the assumption of infinite homogeneous layers and the multi-layered case, is performed. For each case, 2×10^4 realizations

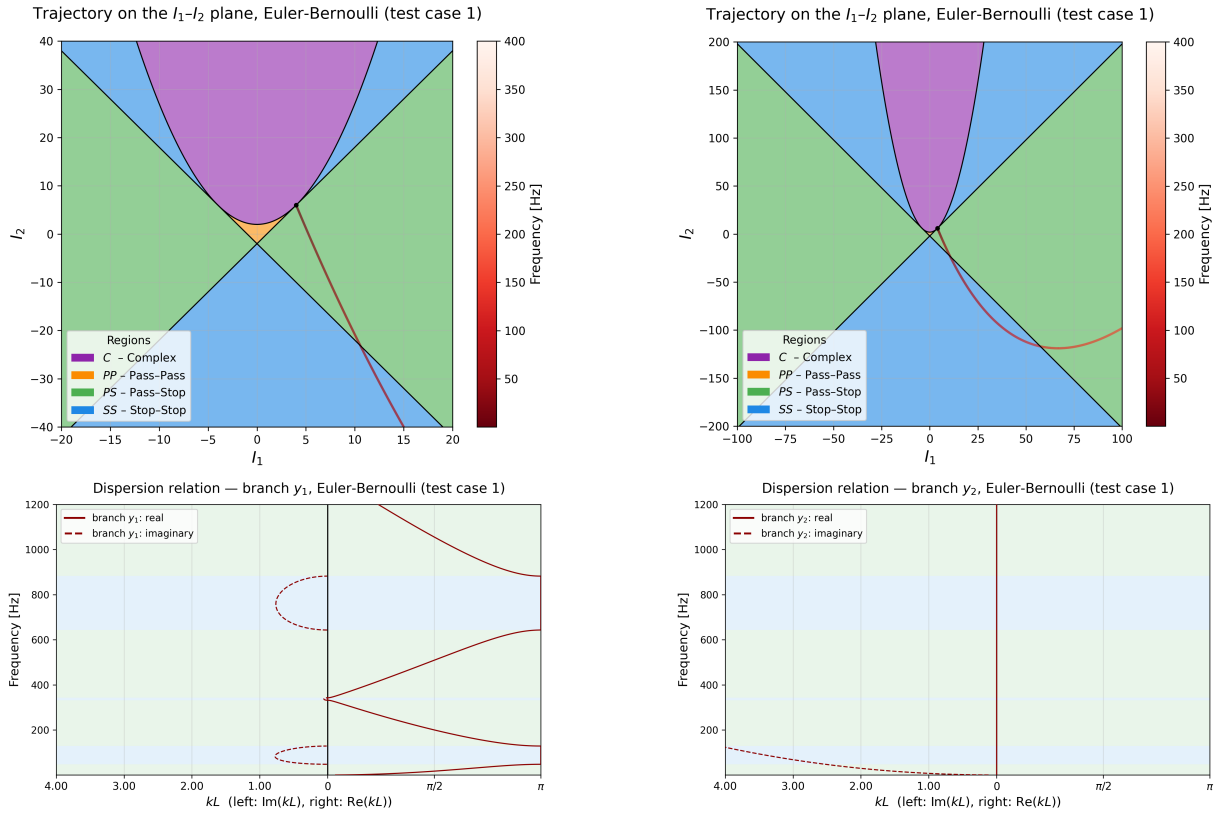

Figure 4: Example of trajectory in the I_1–I_2 space for a bi-layered Euler–Bernoulli beam at two different zoom levels. The dispersion relations associated with the two branches of the problem are reported with colored regions in the background, in correspondence with the regions in the I_1–I_2 space. The trajectories are computed using the following parameters. Layer 1: $E_1 = 3.2 \times 10^{10}\,\mathrm{Pa}$, $\rho_1 = 7850\,\mathrm{kg\,m^{-3}}$, $A_1 = 1.4 \times 10^{-1}\,\mathrm{m^2}$, $I_1 = 6.3 \times 10^{-3}\,\mathrm{m^4}$, $L_1 = 1.35\,\mathrm{m}$. Layer 2: $E_2 = 2.1 \times 10^{11}\,\mathrm{Pa}$, $\rho_2 = 7850, \mathrm{kg\,m^{-3}}$, $A_2 = 1.8 \times 10^{-2}\,\mathrm{m^2}$, $I_2 = 2.9 \times 10^{-3}\,\mathrm{m^4}$, $L_2 = 3.25\,\mathrm{m}$.

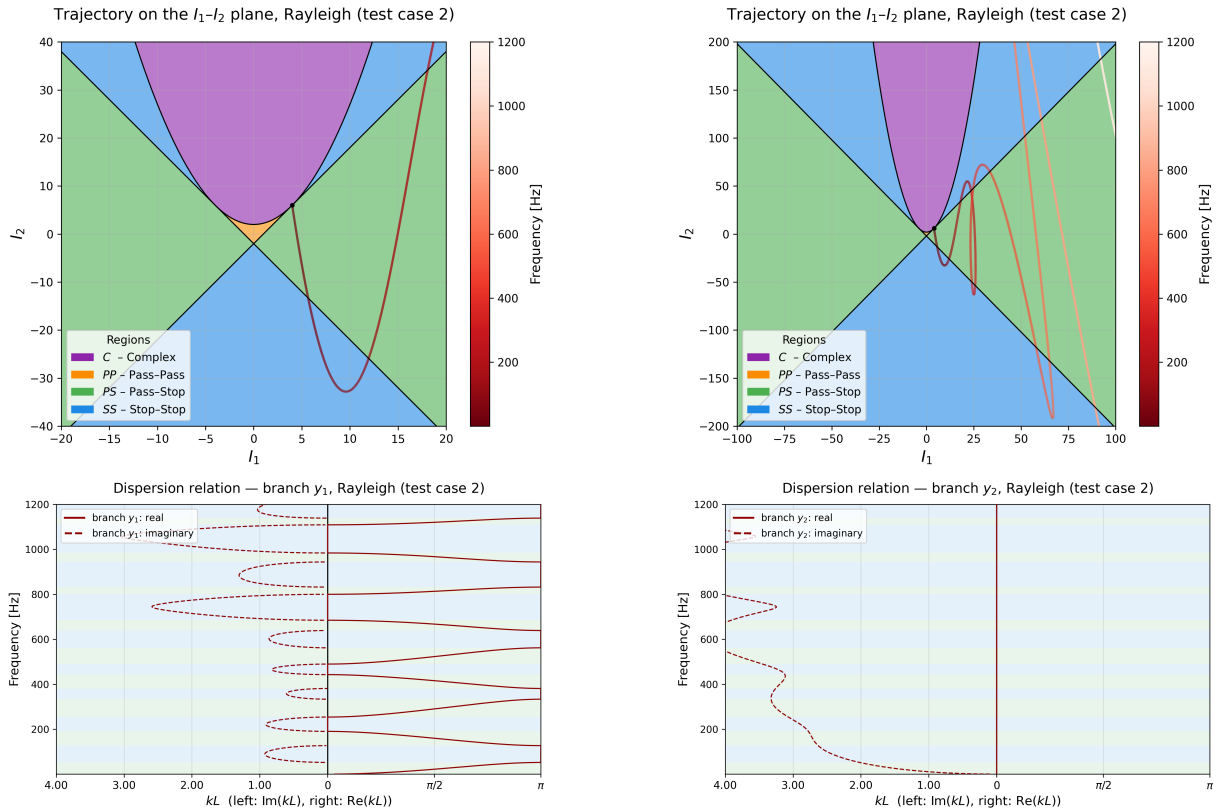

Figure 5: Example of trajectory in the I_1–I_2 space for a bi-layered Rayleigh beam at two different zoom levels. The dispersion relations associated with the two branches of the problem are reported with colored regions in the background, in correspondence with the regions in the I_1–I_2 space. The trajectories are computed using the following parameters. Layer 1: $E_1 = 3.2 \times 10^{10}\,\mathrm{Pa}$, $\rho_1 = 1099\,\mathrm{kg\,m^{-3}}$, $A_1 = 1.0 \times 10^{-1}\,\mathrm{m^2}$, $I_1 = 1.2 \times 10^{-3}\,\mathrm{m^4}$, $L_1 = 1.35\,\mathrm{m}$. Layer 2: $E_2 = 8.53 \times 10^{9}\,\mathrm{Pa}$, $\rho_2 = 7850\,\mathrm{kg\,m^{-3}}$, $A_2 = 1.2 \times 10^{-3}\,\mathrm{m^2}$, $I_2 = 1.2 \times 10^{-2}\,\mathrm{m^4}$, $L_2 = 3.25\,\mathrm{m}$.

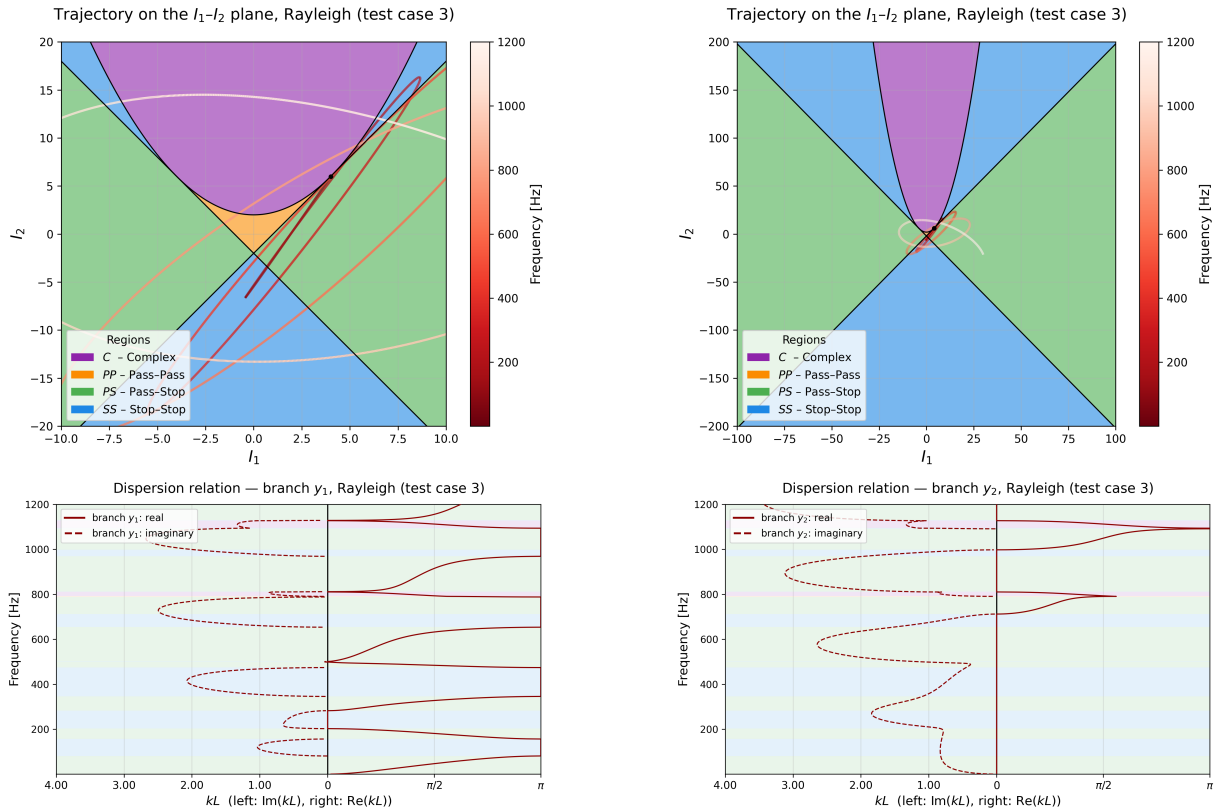

Figure 6: Example of trajectory in the I_1–I_2 space for a bi-layered Rayleigh beam at two different zoom levels. The dispersion relations associated with the two branches of the problem are reported with colored regions in the background, in correspondence with the regions in the I_1–I_2 space. The trajectories are computed using the following parameters. Layer 1: $E_1 = 3.2 \times 10^{10}\,\mathrm{Pa}$, $\rho_1 = 628\,\mathrm{kg\,m^{-3}}$, $A_1 = 1.0 \times 10^{-1}\,\mathrm{m^2}$, $I_1 = 1.2 \times 10^{-2}\,\mathrm{m^4}$, $L_1 = 1.35\,\mathrm{m}$. Layer 2: $E_2 = 8.53 \times 10^{9}\,\mathrm{Pa}$, $\rho_2 = 7850\,\mathrm{kg\,m^{-3}}$, $A_2 = 1.2 \times 10^{-3}\,\mathrm{m^2}$, $I_2 = 1.2 \times 10^{-1}\,\mathrm{m^4}$, $L_2 = 3.25\,\mathrm{m}$.

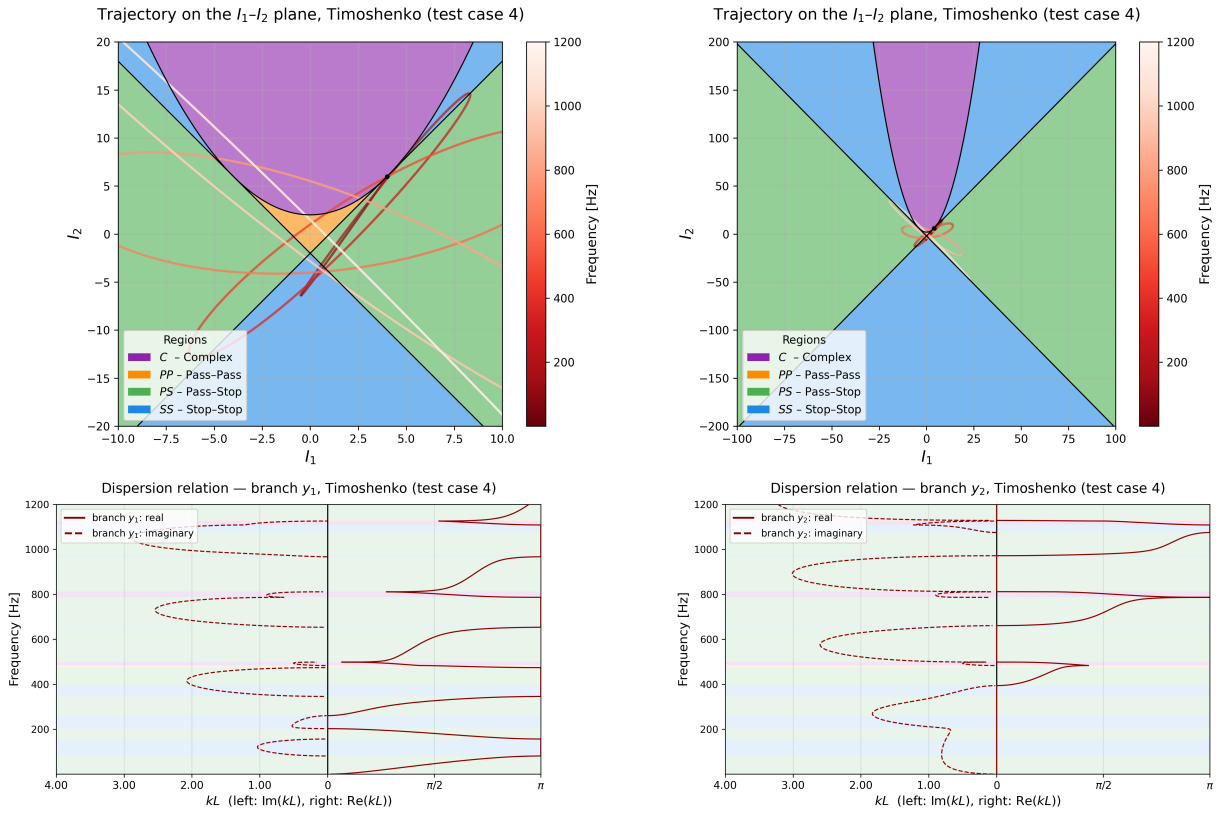

Figure 7: Example of trajectory in the I_1–I_2 space for a bi-layered Timoshenko beam at two different zoom levels. The dispersion relations associated with the two branches of the problem are reported with colored regions in the background, in correspondence with the regions in the I_1–I_2 space. The trajectories are computed using the following parameters. Layer 1: $E_1 = 3.2 \times 10^{10}\,\mathrm{Pa}$, $\rho_1 = 628\,\mathrm{kg\,m^{-3}}$, $A_1 = 1.0 \times 10^{-1}\,\mathrm{m^2}$, $I_1 = 1.2 \times 10^{-2}\,\mathrm{m^4}$, $kGA_1 = 5.0 \times 10^{9}\,\mathrm{N}$, $L_1 = 1.35\,\mathrm{m}$. Layer 2: $E_2 = 8.53 \times 10^{9}\,\mathrm{Pa}$, $\rho_2 = 7850\,\mathrm{kg\,m^{-3}}$, $A_2 = 1.2 \times 10^{-3}\,\mathrm{m^2}$, $I_2 = 1.2 \times 10^{-1}\,\mathrm{m^4}$, $kGA_2 = 5.0 \times 10^{9}\,\mathrm{N}$, $L_2 = 3.25\,\mathrm{m}$.

are generated. The parameter ranges are selected in dimensionless form so as to explore the invariant-plane structure without tying the analysis to a specific physical scale. In this way, the sampling emphasizes the qualitative distribution of the invariants across beam models rather than the response of a particular dimensional benchmark. The parameters $\rho \in [10^{-1}, 10]$, $\omega \in [1, 100]$, $A \in [0.2, 15]$, $I \in [0.02, 5]$, and $E \in [0.05, 15]$ (and $G \in [0.05, 15]$ for the Timoshenko model) are sampled from log-uniform distributions, while the segment lengths are sampled uniformly as $L \in [0.2, 3]$.

For each configuration, the two corresponding invariants I_1 and I_2 have been computed as in eq. (11b). The results in Figure 8, Figure 9, and Figure 10, show points in the $I_1 - I_2$ space, each associated with one configuration. Every point has to be understood as "generating a random trajectory and sampling a random point from it".

It can be observed how in the Euler–Bernoulli case the results are consistent with the conclusions from Section 4.1. Also, for Rayleigh and Timoshenko beams in the multi-layered case the four regions in the $I_1 - I_2$ space are reached. It is however worth highlighting that these simulations are performed over a limited set of configurations, and the absence of points in certain region should not be interpreted automatically as the impossibility of generating a suitable configuration for that region given the model and assumptions considered. More importantly, the choice of parameters used for the study has not been constrained by considerations of practical feasibility.

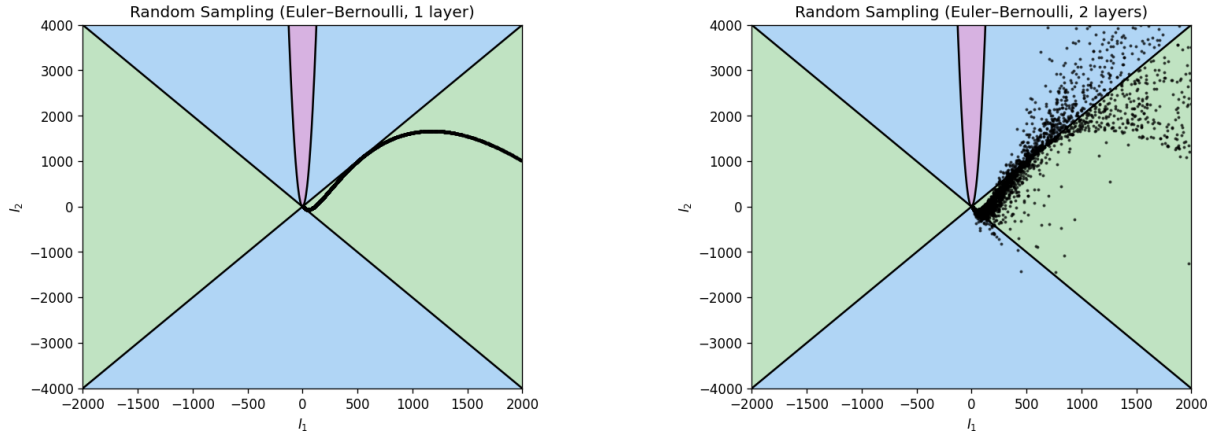

i) homogeneous beams

ii) multi-layered beams

Figure 8: Random sampling of frequencies and trajectories for Euler–Bernoulli beams.

5 Discussion

5.1 Some observations (case $N = 2$, the function $\eta(\omega)$ and trajectory shapes)

The results presented in this work for the general case of arbitrary number of layers N are in agreement with previous results available in the literature. Indeed, in Lee et al. (1990) periodic bi-layered Euler–Bernoulli beams are considered, presenting the fact that one propagation mode is always evanescent, and the formation of bandgaps always depends only on the second mode known *a priori*, analogously to the result derived in this work apart from a reversed sign convention. Also in Carta and Brun (2015) the case of Euler–Bernoulli beams $N = 2$ is presented, explicitly showing trajectories on the $I_1 - I_2$ space, that entirely lie inside the restricted regions Pass-Stop and Stop-Stop.

For Euler–Bernoulli beams, the existence of a single scalar function η that uniquely determines the formation of a bandgap, even for a problem described by two coordinates in the $I_1 - I_2$ space, is identical

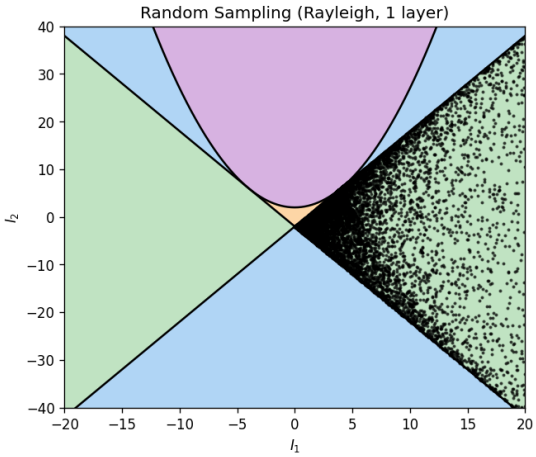

i) homogeneous beams

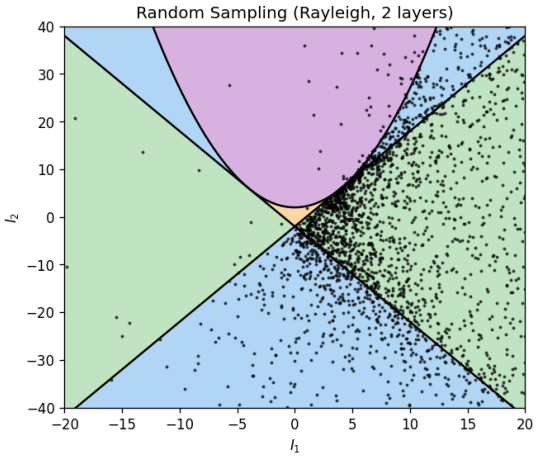

ii) multi-layered beams

Figure 9: Random sampling of frequencies and trajectories for Rayleigh beams.

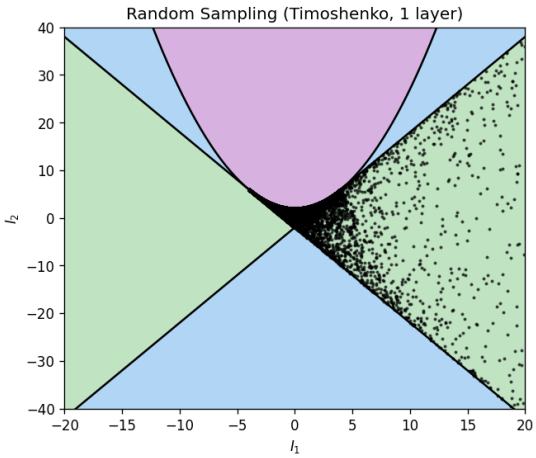

i) homogeneous beams

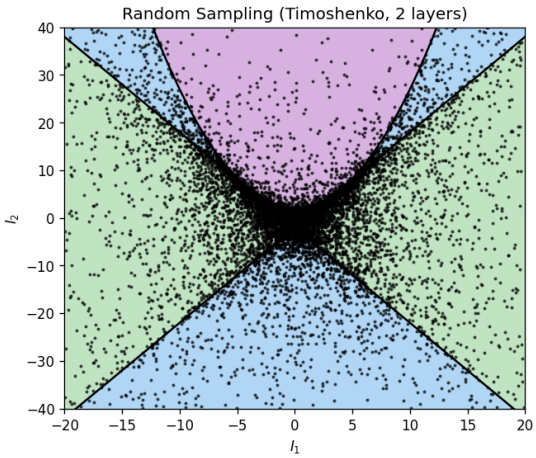

ii) multi-layered beams

Figure 10: Random sampling of frequencies and trajectories for Timoshenko beams.

in spirit to the *half trace function* $\eta(\omega)$ for longitudinal waves in rods considered for example in García-Suárez (2022). Indeed, it turns out that for both cases one wave mode is propagating when $|\eta| < 1$ while conversely a bandgap occurs. This strict analogy should not be interpreted as a coincidence. Indeed, it is known that the transfer matrices for longitudinal waves in rods belong to the symplectic Lie group $\mathrm{Sp}(2, \mathbb{R})$ (Totaro, 2010), hence the spectrum is controlled by only one reciprocal pair of eigenvalues. However, even if the transfer matrices in the Euler–Bernoulli case are in the higher dimensional group $\mathrm{Sp}(4, \mathbb{R})$, there is only one *non-dominant* pair of eigenvalues which controls bandgaps.

Apart from the fact that for Rayleigh (and Timoshenko) beams the constraints in the $I_1 - I_2$ space imposed by Euler–Bernoulli beams are no longer valid, one might also note that in Figure 4, Figure 5, Figure 6 and Figure 7, only for Euler–Bernoulli beams the trajectory is non overlapping, namely never happens that for two different frequencies the same $I_1 - I_2$ value is attained. One could attempt to prove that the function $\omega \to I_1(\omega)$ is guaranteed to be monotonically increasing and unbounded for Euler-Bernoulli beams, consequently a trajectory can never "move to the left" for increasing frequencies, that is what can be observed in both Figure 5, Figure 6 and Figure 7. This is left for future work.

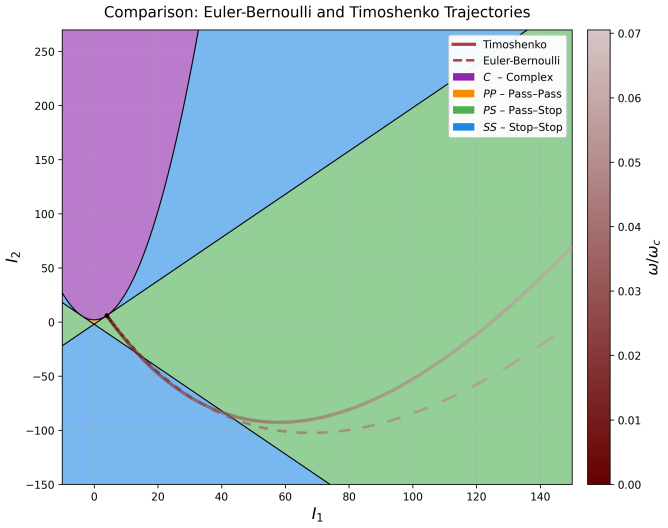

Figure 11: Comparison of trajectories in the I_1–I_2 space for a bi-layered beam modeled using Euler–Bernoulli (dashed black line) and Timoshenko (solid line) theories. The trajectories are computed using identical geometric and material parameters for both layers. Layer 1: $E_1 = 5 \times 10^9\,\mathrm{Pa}$, $\rho_1 = 3200\,\mathrm{kg\,m^{-3}}$, $A_1 = 2.0 \times 10^{-2}\,\mathrm{m^2}$, $I_1 = 4.0 \times 10^{-4}\,\mathrm{m^4}$, $L_1 = 2.35\,\mathrm{m}$, $kGA_1 = 5.0 \times 10^{15}\,\mathrm{N}$. Layer 2: $E_2 = 4.0 \times 10^{10}\,\mathrm{Pa}$, $\rho_2 = 7000\,\mathrm{kg\,m^{-3}}$, $A_2 = 1.0 \times 10^{-2}\,\mathrm{m^2}$, $I_2 = 2.0 \times 10^{-3}\,\mathrm{m^4}$, $L_2 = 2.10\,\mathrm{m}$, $kGA_2 = 7.0 \times 10^{15}\,\mathrm{N}$. The Timoshenko trajectory is colored according to the normalized frequency ω/ω_c. The critical frequency ω_c is defined as $\omega_c = \min_{j=1,2}\left(r_{g,j}^{-1}\sqrt{E_j/\rho_j}\right)$, $r_{g,j} = \sqrt{I_j/A_j}$, so that $\omega/\omega_c = \max_j\left(\omega\, r_{g,j}/\sqrt{E_j/\rho_j}\right)$.

5.2 On the possibility of flexural wave engineering

The plots in Figure 4, Figure 5, Figure 6 or in Figure 7 may convey the idea that designing bandgaps under the Euler-Bernoulli assumptions is futile, given how the unaccounted rotary inertia and shear-bending coupling can perturb the trajectories in $I_1 - I_2$, i.e., change the bandgaps.

The condition for both rotary inertia and shear stiffness to be negligible (Banerjee, 2022; Wang and So, 2015) can be expressed in terms of dimensionless conditions using either λ (the wavelength of the

wave) or ω (its circular frequency):

$$\frac{r_g}{\lambda} \ll 1 \rightarrow \omega \ll \frac{\sqrt{E/\rho}}{r_g}\,, \tag{20}$$

where $r_g = \sqrt{I/A}$ is the "radius of gyration", a characteristic length of the cross-section. This means that for high-frequency bands, sooner or later, the Euler-Bernoulli model will fail to deliver accurate results; The sooner the less slender the beam or the softer the material. This means that at least the first bandgap can be safely studied using the Euler-Bernoulli model, but one must be careful and assess, on a case-by-case basis, when to add the other effects in the beam analysis. To illustrate this point, see Figure 11.

5.3 Extensions to Continuous Profiles

The results derived in this work rely on the assumption of constant property profiles for each transfer matrix T_n. However, given the generality of the results in terms of arbitrary number of layers N, one might be wondering if the validity of the results extends beyond the piecewise constant assumption, for example by considering piecewise-continuous, and in particular continuous, profiles as in Pelat et al. (2019) or Li and Biwa (2020). Can a generic continuous profile be approximated in the piecewise constant sense by N transfer matrices as in Figure 12, arbitrarily improving the approximation taking the limit $N \rightarrow \infty$? Under which regularity assumptions on the profile of the properties in the interval $[0, L]$ can this be done?

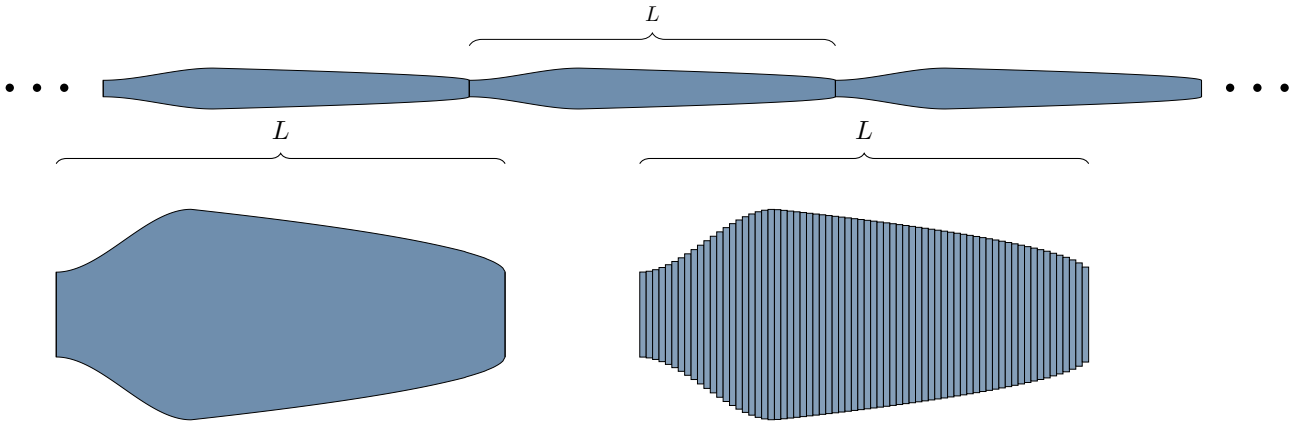

exact profile piecewise-constant approximation ($N = 70$ layers)

Figure 12: Discretization of a continuous profile within a unit cell with a piecewise constant one.

Answering such questions through a detailed analysis falls beyond the scope of this work. However, it is worth noting that in previous work across various domains, the mathematical properties of symplecticity or entry-wise positivity of matrices solutions of a first order matrix ODE equivalent to the one in eq. (4) are still verified without any piecewise-constant assumption on $H(x)$. Concerning symplecticity, in Iserles and Nørsett (1999) it is mentioned that matrices which are solution of an equation equivalent to eq. (4) belong to some Lie group whenever $H(x)$ belongs to the corresponding Lie algebra and the function $H(x)$ fulfills the mild regularity assumption of Lipschitz continuity. For positivity, instead, it is presented in the literature (Hirsch, 1985; Benaïm et al., 2024) that nonnegative matrices $H(x)$ lead to entrywise positive matrix solutions by only assuming finite left and right limits at discontinuities of $H(x)$ within some periodically repeated profiles. Finally, it can be observed that the results derived in this work in terms of existence of a fully evanescent branch k_2 and one possibly propagating or evanescent branch k_1 are in accordance with the results in Li and Biwa (2020) for arbitrary contour profiles.

6 Conclusion

In this work, by means of a combined use of the symplectic properties and the notion of dominant eigenvalue, several spectral properties have been determined for transfer matrices of multi-layered Euler–Bernoulli beams with arbitrary number of layers and parameters. Implications in terms of possible wave propagation regimes have been presented, guaranteeing that only two wave propagation modes are possible, as long as the existence of a single function that serves as a criterion to identify bandgaps, regardless of the wave frequency or medium configuration. This result can offer advantages towards improved approaches in bandgap engineering and optimization by identifying a unique objective function to be evaluated while performing parametric selection. For Rayleigh and Timoshenko beams it has been shown how the identification of an analogous function is not possible, also investigating differences in the trajectories in the space of the invariants compared to Euler–Bernoulli beams and their implications in terms of possible wave propagation regimes. Comparisons with previous studies have been performed, showing strong analogies between longitudinal waves in rods and flexural waves in Euler–Bernoulli beams. The results derived in this work, despite their generality, rely on a set of idealized assumptions. Examining their robustness in presence of perturbations, such as finite length media, viscoelastic effects, or non-exact periodicity, falls beyond the scope of this manuscript. Even though these results might serve as a foundation to tackle the case of continuous beam property profiles, such as those considered in Pelat et al. (2019); Li and Biwa (2020), a rigorous development of the topic is left for future work. Various questions on the emergence of bandgaps under different beam modeling assumptions are also left for future investigations, for example understanding which elements determine a transition of the shape of the trajectories in the $I_1 - I_2$ space from more "symmetric and overlapping" in the Timoshenko or Rayleigh case towards more "nonsymmetric and monotone" in Euler–Bernoulli beams, and how the type of "collisions" of eigenvalues on the unit circle, as studied in Yakubovich and Starzhinskii (1975), varies accordingly. Finally, given that "*waves always behave in a similar way, whether they are longitudinal or transverse, elastic or electric*" (Brillouin, 1953), it cannot be excluded that the scope of this work might provide novel insights beyond mechanical waves in beams.

Acknowledgements

The authors gratefully acknowledge support from the Swiss National Science Foundation via Ambizione Grant 216341. The authors are also thankful to Prof. Anna Pandolfi (Politecnico di Milano) and Dr. Guillaume Anciaux (EPFL) for stimulating discussions.

Material Availability

The code (Python) to reproduce the figures and results of this manuscript is available via correspondence with the authors under reasonable request. The Supplementary Material will be made available upon publication and it can already be obtained via correspondence with the second author (`joaquin.garciasuarez@epfl.ch`).

References

Banerjee, J. R. (2022). Free vibration of timoshenko–ehrenfest beams and frameworks using frequency-dependent mass and stiffness matrices. *Journal of Vibration and Acoustics*, 144(6):064501.

Benaïm, M., Lobry, C., Sari, T., and Strickler, E. (2024). When can a population spreading across sink habitats persist? *Journal of Mathematical Biology*, 88(19):1–56.

Berman, A. and Plemmons, R. J. (1994). *Nonnegative Matrices in the Mathematical Sciences*, volume 9 of *Classics in Applied Mathematics*. Society for Industrial and Applied Mathematics.

Bloch, F. (1929). Über die Quantenmechanik der Elektronen in Kristallgittern. *Zeitschrift für Physik*, 52:555–600.

Brillouin, L. N. (1953). *Wave Propagation in Periodic Structures: Electric Filters and Crystal Lattices*. Dover Publications, 2nd edition. Originally published 1946 (McGraw-Hill).

Carta, G. and Brun, M. (2015). Bloch–Floquet waves in flexural systems with continuous and discrete elements. *Mechanics of Materials*, 87:11–26.

Dai, S., Gao, H., Mao, J., Gao, P., and Qu, Y. (2024). Flexural wave compression behaviors of programmable graded piezoelectric meta-beams. *International Journal of Mechanical Sciences*, 283:109743.

de Gosson, M. A. (2006). *Symplectic Geometry and Quantum Mechanics*, volume 166 of *Operator Theory: Advances and Applications*. Birkhäuser Basel.

Doyle, J. F. (2020). *Wave Propagation in Structures*. Springer, Cham, 3 edition.

García-Suárez, J. (2022). Harmonic decomposition of the trace of 1d transfer matrices in layered media. *Journal of the Mechanics and Physics of Solids*, 163.

González-Carbajal, J., Lemm, M., and Garcia-Suarez, J. (2025). On the lowest-frequency bandgap of 1d phononic crystals. *European Journal of Mechanics - A/Solids*, 109:105466.

Hall, B. C. (2015). *Lie Groups, Lie Algebras, and Representations: An Elementary Introduction*, volume 222 of *Graduate Texts in Mathematics*. Springer International Publishing, second edition edition.

Hirsch, M. W. (1985). Systems of differential equations that are competitive or cooperative ii: Convergence almost everywhere. *SIAM Journal on Mathematical Analysis*, 16(3):423–439.

Horn, R. A. and Johnson, C. R. (2012). *Matrix Analysis*. Cambridge University Press, 2 edition.

Hussein, M. I., Leamy, M. J., and Ruzzene, M. (2014). Dynamics of phononic materials and structures: Historical origins, recent progress, and future outlook. *Applied Mechanics Reviews*, 66(4).

Iserles, A. and Nørsett, S. P. (1999). On the solution of linear differential equations in Lie groups. *Philosophical Transactions of the Royal Society of London. Series A: Mathematical, Physical and Engineering Sciences*, 357(1754):983–1019.

Judson, T. W. and Beezer, R. A. (2022). Abstract algebra: Theory and applications. Open-access textbook, GNU Free Documentation License; Accessed: 2026-1-4.

Kittel, C. (2004). *Introduction to Solid State Physics*. John Wiley & Sons, 8 edition.

Leckie, F. and Pestel, E. (1960). Transfer-matrix fundamentals. *International Journal of Mechanical Sciences*, 2(3):137–167.

Lee, S. Y., Ke, H. Y., and Kao, M. J. (1990). Flexural waves in a periodic beam. *Journal of Applied Mechanics*, 57(3):779–783.

Li, P. and Biwa, S. (2020). Flexural waves in a periodic non-uniform Euler–Bernoulli beam: Analysis for arbitrary contour profiles and applications to wave control. *International Journal of Mechanical Sciences*, 188.

Lim, C. W. and Xu, X. S. (2010). Symplectic elasticity: Theory and applications. *Applied Mechanics Reviews*, 63(5).

Liu, L. and Hussein, M. I. (2011). Wave motion in periodic flexural beams and characterization of the transition between bragg scattering and local resonance. *Journal of Applied Mechanics*, 79(1):011003.

Mead, D. J. (1975). Wave propagation and natural modes in periodic systems: II. Multi-coupled systems, with and without damping. *Journal of Sound and Vibration*, 40(1):19–39.

Pelat, A., Gallot, T., and Gautier, F. (2019). On the control of the first bragg band gap in periodic continuously corrugated beam for flexural vibration. *Journal of Sound and Vibration*, 446:249–262.

Price, H., Chong, Y., Khanikaev, A. B., Schomerus, H., Maczewsky, L. J., Kremer, M., Heinrich, M., Szameit, A., Zilberberg, O., Yang, Y., Zhang, B., Alù, A., Thomale, R., Carusotto, I., St-Jean, P., Amo, A., Dutt, A., Yuan, L., Fan, S., Yin, X., Peng, C., Ozawa, T., and Blanco-Redondo, A. (2022). Roadmap on topological photonics. *Journal of Physics: Photonics*, 4(3).

Renno, J. (2025). On the optimization of band gaps in periodic waveguides. *Journal of Vibration Engineering & Technologies*, 13:625.

Romeo, F. (2012). Map-based approaches for periodic structures. In Romeo, F. and Ruzzene, M., editors, *Wave Propagation in Linear and Nonlinear Periodic Media*, volume 540 of *CISM Courses and Lectures*, pages 161–256. Springer.

Romeo, F. and Luongo, A. (2002). Invariant representation of propagation properties for Bi-coupled periodic structures. *Journal of Sound and Vibration*, 257(5):869–886.

Stephen, N. G. (2006). Transfer matrix analysis of the elastostatics of one-dimensional repetitive structures. *Proceedings of the Royal Society A: Mathematical, Physical and Engineering Sciences*, 462(2072):2245–2270.

Timoshenko, S. P. (1930). *Strength of Materials*. D. Van Nostrand Company.

Totaro, B. (2010). Lie group, lie algebra and their representations. Lecture notes, typeset by Aaron Chan. Accessed: 2025-12-3.

Wang, S., Shao, N., Chen, H., Chen, J., Qian, H., Wu, Q., Duan, H., Alù, A., and Huang, G. (2025). Experimental realization of temporal refraction and reflection in elastic beams. *Nature Communications*, 16:9520.

Wang, X. and So, R. (2015). Timoshenko beam theory: A perspective based on the wave-mechanics approach. *Wave Motion*, 57:64–87.

Yakubovich, V. A. and Starzhinskii, V. M. (1975). *Linear Differential Equations with Periodic Coefficients*. John Wiley & Sons / Halsted Press, New York.

Zhang, J., Hu, G., Tang, H., and Yang, Y. (2025). Broadband and tunable vibration suppression via piezoelectric-abh meta-beam. *International Journal of Mechanical Sciences*, 296:110312.

Zhang, X., Zhang, J., Xu, C., Rong, J., Hu, N., Deng, M., and Zhang, C. (2024). Inverse-designed flexural wave metamaterial beams with thermally induced tunability. *International Journal of Mechanical Sciences*, 267:109007.